ELECTRONICS AND ELECTRICAL ENGINEERING
ISSN 1392 – 1215 *2011. No. 10(116)*
ELEKTRONIKA IR ELEKTROTECHNIKA

ELECTRICAL ENGINEERING
T 190
ELEKTROS INŽINERIJA

Numerical Analysis of Electric Wind in Corona Field

P. Marciulionis, S. Zebrauskas
Department of Electrical Engineering, Kaunas University of Technology,
Studentų st. 48, LT-51367 Kaunas, Lithuania, phone: +370 37 300268, e-mails: stasys.zebrauskas@ktu.lt, povilas.marciulionis@ktu.lt

crossref http://dx.doi.org/10.5755/j01.eee.116.10.871

Introduction

Two-dimensional digital model for analysis of direct current corona field and induced electrohydrodynamic air flow field in wire-to-plane electrode system is presented. The model based on the finite-difference method in polar coordinate system for corona field computation is suitable to use in usual personal computers. Results of computation of current-voltage discharge characteristic are compared with experimental one. The digital model of electrohydrodynamic air flow field consists of finite-difference approximation of the Navier-Stokes equation and the continuity equation in Cartesian coordinates. Digital velocity values are checked experimentally. Movement of charges in outer zone of the discharge is complicated due to drag of neutral air molecules. This is the reason of electrohydrodynamic flow rise named as electric wind. Electric wind phenomenon can be used for heat and mass enhancement, in ionic air cleaners etc. Many results of experimental and theoretical research are published [1, 2]. Because of high voltage conditions in the discharge gap authors use for experimental research laser-Doppler anemometers, particle image velocimetry systems or hot-wire anemometers [3–5]. Theoretical research is related to simultaneous analysis of electric field in the electrode system with direct-current corona discharge and air flow field in the system. Analytical study of this complex problem can be performed only for one-dimensional field of coaxial electrode system. Analysis of the complex field in all practical electrode systems, such as wire-to-plate, pin-to-plate etc, is available only by use of numerical methods.

Modeling direct current corona field

We use the system of corona field equations in wire-to-plane electrode system reduced to the Poisson's equation and the charge conservation equation. The finite difference approximation of the Poisson's equation in polar system of coordinates is the following [6]

$$\frac{2V_{\mathrm{P}}}{a_{\mathrm{P}}^2+a_{\mathrm{P}}a_{\mathrm{R}}}+\frac{2V_{\mathrm{R}}}{a_{\mathrm{R}}^2+a_{\mathrm{P}}a_{\mathrm{R}}}+\frac{2V_{\mathrm{Q}}}{a_{\mathrm{Q}}^2+a_{\mathrm{Q}}a_{\mathrm{S}}}+\frac{2V_{\mathrm{S}}}{a_{\mathrm{S}}^2+a_{\mathrm{Q}}a_{\mathrm{S}}}+\frac{a_S V_{\mathrm{Q}}}{r_1(a_{\mathrm{Q}}^2+a_{\mathrm{Q}}a_{\mathrm{S}})}-$$

$$-\frac{a_Q V_{\mathrm{S}}}{r_1(a_{\mathrm{S}}^2+a_{\mathrm{Q}}a_{\mathrm{S}})}-V_{\mathrm{O}}\left(\frac{2}{a_{\mathrm{Q}}a_S}+\frac{2}{a_{\mathrm{R}}a_{\mathrm{P}}}+\frac{a_{\mathrm{S}}^2-a_{\mathrm{Q}}^2}{r_1\left(a_{\mathrm{Q}}a_{\mathrm{S}}^2+a_{\mathrm{S}}a_{\mathrm{Q}}^2\right)}\right)=-\frac{\rho_{\mathrm{O}}}{\varepsilon}. \quad (1)$$

The partial derivatives of the charge conservation equation

$$\frac{\partial\rho}{\partial r}\cdot\frac{\partial V}{\partial r}+r\frac{\partial\rho}{\partial\varphi}\cdot r\frac{\partial V}{\partial\varphi}=\frac{\rho^2}{\varepsilon} \quad (2)$$

are of the form:

$$\frac{\partial V}{\partial r}=-\frac{V_{\mathrm{S}}a_{\mathrm{Q}}}{a_{\mathrm{S}}\left(a_{\mathrm{Q}}+a_{\mathrm{S}}\right)}+\frac{V_{\mathrm{Q}}a_{\mathrm{S}}}{a_{\mathrm{Q}}\left(a_{\mathrm{Q}}+a_{\mathrm{S}}\right)}+\frac{V_{\mathrm{O}}\left(a_{\mathrm{Q}}-a_{\mathrm{S}}\right)}{a_{\mathrm{Q}}a_{\mathrm{S}}}, \quad (3)$$

$$\frac{r\partial V}{\partial\varphi}=-\frac{V_{\mathrm{P}}a_{\mathrm{R}}}{a_{\mathrm{P}}\left(a_{\mathrm{P}}+a_{\mathrm{R}}\right)}+\frac{V_{\mathrm{R}}a_{\mathrm{P}}}{a_{\mathrm{R}}\left(a_{\mathrm{P}}+a_{\mathrm{R}}\right)}+\frac{V_{\mathrm{O}}\left(a_{\mathrm{P}}-a_{\mathrm{R}}\right)}{a_{\mathrm{P}}a_{\mathrm{R}}}, \quad (4)$$

$$\frac{\partial\rho}{\partial r}=\frac{\rho_{\mathrm{Q}}a_{\mathrm{S}}}{a_{\mathrm{Q}}\left(a_{\mathrm{Q}}+a_{\mathrm{S}}\right)}-\frac{\rho_{\mathrm{S}}a_{\mathrm{Q}}}{a_{\mathrm{S}}\left(a_{\mathrm{Q}}+a_{\mathrm{S}}\right)}+\frac{\rho_{\mathrm{O}}\left(a_{\mathrm{Q}}-a_{\mathrm{S}}\right)}{a_{\mathrm{Q}}a_{\mathrm{S}}}, \quad (5)$$

$$\frac{r\partial\rho}{\partial\varphi}=-\frac{\rho_{\mathrm{P}}a_{\mathrm{R}}}{a_{\mathrm{P}}\left(a_{\mathrm{P}}+a_{\mathrm{R}}\right)}+\frac{\rho_{\mathrm{R}}a_{\mathrm{P}}}{a_{\mathrm{R}}\left(a_{\mathrm{P}}+a_{\mathrm{R}}\right)}-\frac{\rho_{\mathrm{O}}\left(a_{\mathrm{P}}-a_{\mathrm{R}}\right)}{a_{\mathrm{P}}a_{\mathrm{R}}}, \quad (6)$$

where potential is represented by V and space charge density correspondingly by ρ. Distances from the central node of polar grid O to the neighbor nodes P, Q, R and S are denoted by a_{P}, a_{Q}, a_{R} and a_{S}. Boundary conditions for potential are of Dirichlet and Neumann type. Boundary condition for space charge density on the surface of the wire is determined iteratively until Kaptzov's condition is established [7]. The number of nodes in polar grid is 518

for the values of geometrical dimensions of the electrode system (Fig. 1) r_0 = 0,05 mm and h = 12,0 mm.

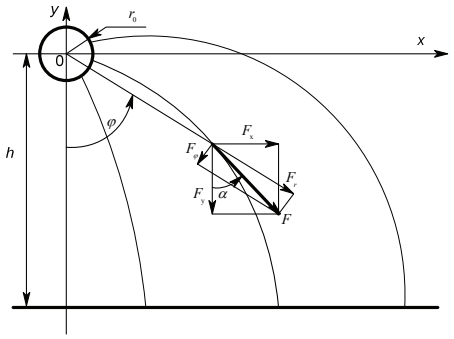

Fig. 1. Coulomb force components

Components of the Coulomb force per unit volume are determined as the product of space charge density and the field strength:

$$F_r = \rho E_r = -\rho \frac{\partial V}{\partial r}, \quad (7)$$

$$F_\varphi = \rho E_\varphi = -\frac{\rho}{r}\frac{\partial V}{\partial \varphi}. \quad (8)$$

Correctness of the model is checked by comparison of the numerical solution of Laplace's equation with analytical solution of an electrostatic field in wire-to-plane electrode system. Average difference between numerical and analytical values of electrostatic field potential on the axis of symmetry (x = 0) is 0,2 % for the number of nodes of polar grid n = 518. Additional test of the numerical corona field model is comparison of numerical data of the current-voltage characteristic with the experimental one.

Maximum difference between numerical and experimental values of linear current density corresponding to the voltage value U = 7,0 kV is 150 μA/m. Spatial components of Coulomb force calculated in rectangular coordinate system is shown in Fig. 2.

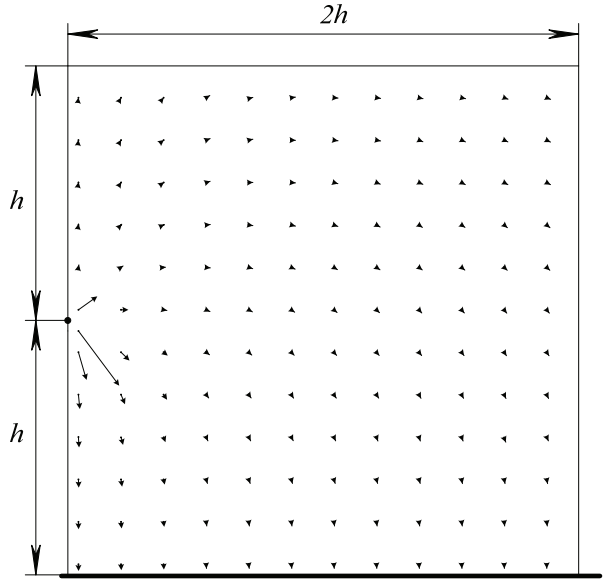

Fig. 2. Spatial force vectors, recounted by rectangular grid force projections in elements of rectangular grid

Numerical model of electro hydrodynamic air flow field

Electrohydrodynamic air flow is determined by the system of equations comprising of the Navier-Stokes and flow continuity equations. Emitting electrode with the ionization zone cross section area is negligible in comparison with an overall area of the field therefore the wire electrode can be represented as a point. Cartesian system of coordinates can be used to reduce the number of nodes. Finite-difference approximation of the Navier-Stokes and the flow continuity equations for this system of coordinates contains the Coulomb force components F_x, F_y and the flow velocity components w_x, w_y [7]:

$$w_{x\mathrm{C}}^{(\tau+1)} = \left(\frac{F_x}{\rho_v} + \nu\left(\frac{w_{x\mathrm{P}}}{a^2} + \frac{w_{x\mathrm{R}}}{a^2} + \frac{w_{x\mathrm{Q}}}{a^2} + \frac{w_{x\mathrm{S}}}{a^2} - \frac{4w_{x\mathrm{C}}}{a^2}\right) - w_{xO}\left(\frac{w_{x\mathrm{C}} - w_{x\mathrm{P}}}{a}\right) - w_{y\mathrm{O}}\left(\frac{w_{x\mathrm{C}} - w_{x\mathrm{S}}}{a}\right)\right)\cdot\Delta\tau + w_{x\mathrm{C}}^{(\tau)}, \quad (9)$$

$$w_{y\mathrm{C}}^{(\tau+1)} = \left(a_y + \frac{F_y}{\rho_v} + \nu\left(\frac{w_{y\mathrm{P}}}{a^2} + \frac{w_{y\mathrm{R}}}{a^2} + \frac{w_{y\mathrm{Q}}}{a^2} + \frac{w_{y\mathrm{S}}}{a^2} - \frac{4w_{y\mathrm{O}}}{a^2}\right) - w_{xO}\left(\frac{w_{y\mathrm{C}} - w_{y\mathrm{P}}}{a}\right) - w_{y\mathrm{O}}\left(\frac{w_{y\mathrm{C}} - w_{y\mathrm{S}}}{a}\right)\right)\cdot\Delta\tau + w_{y\mathrm{C}}^{(\tau)}, \quad (10)$$

$$\frac{w_{y\mathrm{C}} - w_{y\mathrm{S}}}{a} - \frac{w_{x\mathrm{P}} - w_{x\mathrm{R}}}{a} = 0, \quad (11)$$

where $w_{x\mathrm{C}}^{(\tau+1)}$ is the velocity x component value of new iteration, $w_{x\mathrm{C}}^{(\tau)}$ is the value of previous iteration, $w_{x\mathrm{P}}$, $w_{x\mathrm{R}}$, $w_{x\mathrm{S}}$, $w_{x\mathrm{Q}}$ are the x components of velocities in the neighbour nodes, $w_{x\mathrm{O}}$ is the x axis component of average velocity in the square (Fig. 3), $\Delta\tau$ - variation of time between iterations, a – distance between nodes, regular in all the grid (a = 2 mm for Fig. 4).

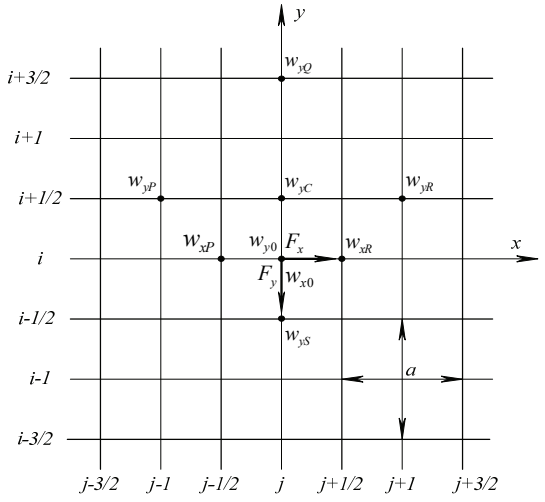

Fig. 3. Computational grid with square elements

It is clear from Fig. 4 and Fig. 5 that Coulomb force strength has an influence to air velocity, but almost no influence to vectors direction, because the ratio of spatial

force components vary insignificantly, only changes their module.

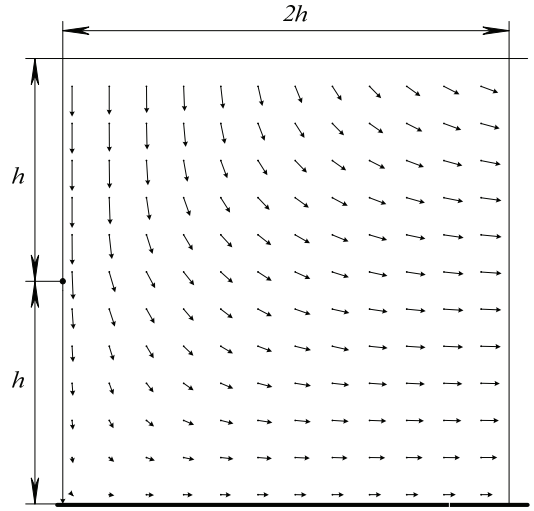

Fig. 4. Electrohydrodynamic air flow distribution in the electrode system for h = 12 mm

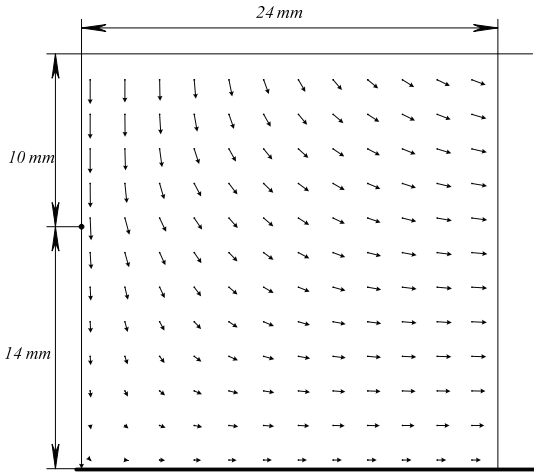

Fig. 5. Electrohydrodynamic air flow distribution in the electrode system when wire is located 14 mm from the plane

Dependence of the air flow velocity in the points of the line x = 2 mm = const upon the distance from the plane electrode is given in Fig. 6. Maximum value of air flow velocity above the wire is approximately 4 m/s.

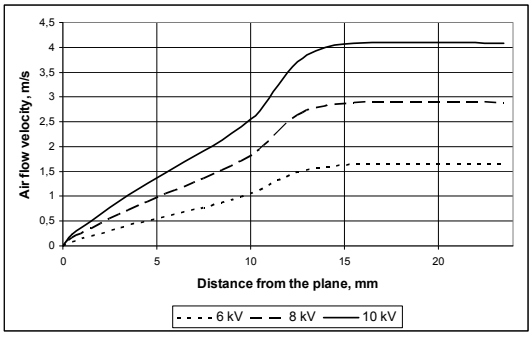

Fig. 6. Air flow velocity at first column away from the axis of symmetry for various wire voltages

Dependence of the air flow velocity in the points of the line y = –10 mm = const upon the distance from the axis of symmetry is given in Fig. 7. Maximum value of air flow velocity near the surface of the plane electrode is 1,5 m/s.

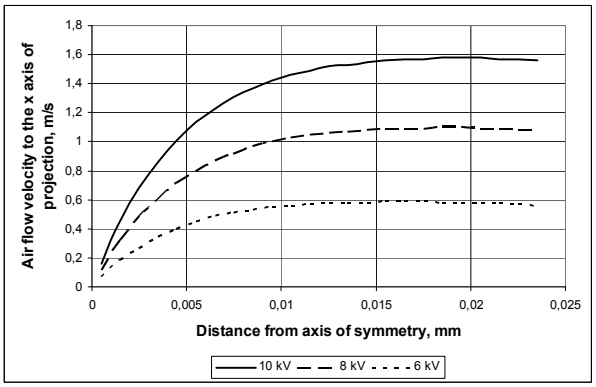

Fig. 7. Air flow velocity on the first line above the plane for various wire voltages

The growth of the volume flow-rate with the variation of coordinate y in the plane x = 24 mm = const is presented in Fig. 8. An overall volume flow-rate through this plane is $60 \cdot 10^{-3}$ m^3/s.

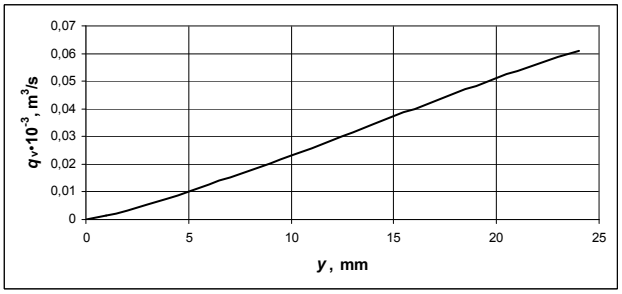

Fig. 8. Growth of the volume flow-rate with variation of y coordinate in the plane x = 24 mm = const

The similar graphic for the plane y = 24 mm = const is given in Fig.9. Data given in Fig. 4, Fig. 8 and Fig 9 correspond to the discharge voltage U = 10 kV.

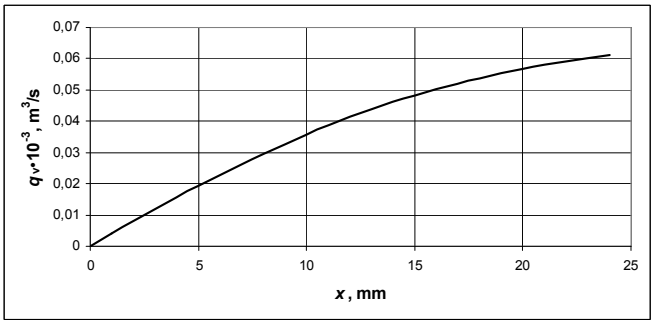

Fig. 9. Growth of the volume flow-rate with variation of x coordinate in the plane y = 24 mm = const

Hot-wire anemometer DO 9847K is used for experimental test of computed data. The diameter of the anemometer probe is 8 mm whereas the spacing between electrodes is 12 mm. Therefore it is no possibility to measure an air flow velocity in the volume between electrodes for the risk of spark discharge and essential distortion not only the corona field, but also the air flow field. Measured value of the airflow velocity in the point x = 60 mm at the surface of plane electrode is 1,02 m/s, and the numerical value is 1,57 m/s, the difference between the

results is 35 %. Coincidence of computed and measured results is only qualitative. This is in agreement with the results of other researchers [3].

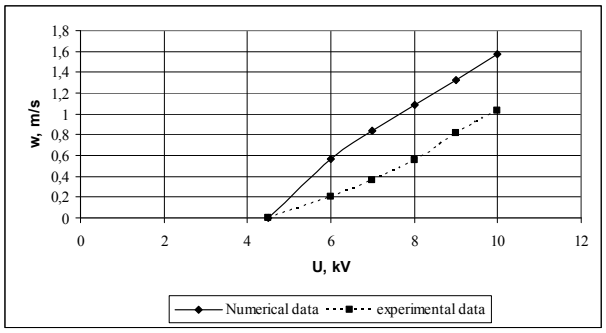

Fig. 10. Experimental and computed air flow velocities dependence upon corona discharge voltage in the point of measurement

Conclusions

Polar grid is used for computation of corona field to reduce the number of nodes in computational area at the sufficient amount of information on the distribution of the field quantities near the emitting electrode.

Two-dimensional numerical model of direct current corona field analysis in wire-to-plane electrode system is based upon the finite-difference method in polar system of coordinates.

It is investigated that Coulomb force strength has an influence to air velocity, but almost no influence to vectors direction, because the ratio of spatial force components vary insignificantly, only changes their module.

Maximum value of air flow velocity above the wire corresponding to the U = 10 kV is approximately 4 m/s. Maximum value of the total volume flow-rate is near the $60 \cdot 10^{-3}$ m^3/s at the mentioned conditions.

Measured and computed values of air flow velocities coincide qualitatively because of the difference between measured and computed values totals about 30%.

References

1. **Jones J. E.** On Corona–Induced Gas Motion and Heating I: Field Equations, Modelling and Vortex Formation // Journal of Electrostatics, 2008. – Vol. 66. – P. 84–93.
2. **Zhao L., Adamiak K.** EHD Flow in Air Produced by Electric Corona Discharge in Pin–Plate Configuration // Journal of Electrostatics, 2005. – Vol. 63. – No. 3–4. – P. 337–350.
3. **Farnoosh N., Adamiak K., Castle G. S. P.** 3–D Numerical Analysis of EHD Turbulent Flow and Mono–disperse Charged Particle Transport and Collection in a Wire–plate ESP // Journal of Electrostatics, 2010. – Vol. 68. – No. 6. – P. 513–522.
4. **Kawamoto H., Yasuda H., Umezu S.** Flow Distribution and Pressure of Air due to Ionic Wind in Pin–to–Plane Corona Discharge System // Journal of Electrostatics, 2006. – Vol. 64. – No. 6. – P. 400–407.
5. **Morozionkov J., Virbalis J. A.** Shielding of Electric Reactor Magnetic Field // Electronics and Electrical Engineering. – Kaunas: Technologija, 2009. – No 8(96). – P. 13–18.
6. **Marčiulionis P., Žebrauskas S.** Numerical Analysis of Spatial Force Components in Direct Current Corona Field // Electronics and Electrical Engineering. – Kaunas: Technologija, 2009. – No. 8(88). – P. 3–8.
7. **Zhao L., Adamiak K.** Numerical Simulation of the Electrohydrodynamic Flow in a Single Wire–Plate Electrostatic Precipitator // IEEE Transactions on Industry Applications, 2008. – Vol. 44. – No. 3. – P. 683–691.

Received 2011 06 28
Accepted after revision 2011 10 03

P. Marciulionis, S. Zebrauskas. Numerical Analysis of Electric Wind in Corona Field // Electronics and Electrical Engineering. – Kaunas: Technologija, 2011. – No. 10(116). – P. 15–18.

Two-dimensional digital model for analysis of direct current corona field and induced electrohydrodynamic air flow field in wire-to-plane electrode system is presented. The model based on the finite-difference method in polar coordinate system for corona field computation is suitable to use in usual personal computers. Results of computation of current-voltage discharge characteristic are compared with experimental one. The digital model of electrohydrodynamic air flow field consists of finite-difference approximation of the Navier-Stokes equation and the continuity equation in Cartesian coordinates. Digital velocity values are checked experimentally. Ill. 10, bibl. 7 (in English; abstracts in English and Lithuanian).

P. Marčiulionis, S. Žebrauskas. Vainikinio išlydžio elektrinio vėjo skaitinė analizė // Elektronika ir elektrotechnika. – Kaunas: Technologija, 2011. – Nr. 10(116). – P. 15–18.

Analizuojamas elektrodų sistemos „laidas šalia plokštumos“ dvimačio vienpolio vainikinio išlydžio elektrinio lauko ir jo sukelto oro tekėjimo lauko analizės skaitinis modelis. Vainikinio išlydžio elektrinis laukas skaičiuojamas baigtinių skirtumų metodu polinėje koordinačių sistemoje. Skaitinio modeliavimo rezultatai yra palyginti su eksperimento rezultatais. Oro tekėjimo lauko lygčių sistemos skaitinį modelį sudaro Naviero ir Stokeso, taip pat tolydumo lygties skirtuminė aproksimacija Dekarto koordinačių sistemoje. Il. 10, bibl. 7 (anglų kalba; santraukos anglų ir lietuvių k.).